

CP_HDR: A feature point detection and description library for LDR and HDR images

Artur Santos Nascimento*, Valter Guilherme Silva de Souza,
Daniel Oliveira Dantas, Beatriz Trinchão Andrade

Departamento de Computação, Universidade Federal de Sergipe (UFS), São Cristóvão, Brazil
{artur.nascimento, vgssouza, ddantas, beatriz}@dcomp.ufs.br

Abstract—In computer vision, *characteristics* refer to image regions with unique properties, such as corners, edges, textures, or areas with high contrast. These regions can be represented through feature points (FPs). FP detection and description are fundamental steps to many computer vision tasks. Most FP detection and description methods use low dynamic range (LDR) images, sufficient for most applications involving digital images. However, LDR images may have saturated pixels in scenes with extreme light conditions, which degrade FP detection. On the other hand, high dynamic range (HDR) images usually present a greater dynamic range but FP detection algorithms do not take advantage of all the information in such images. In this study, we present a systematic review of image detection and description algorithms that use HDR images as input. We developed a library called CP_HDR that implements the Harris corner detector, SIFT detector and descriptor, and two modifications of those algorithms specialized in HDR images, called SIFT for HDR (SfHDR) and Harris for HDR (HfHDR). Previous studies investigated the use of HDR images in FP detection, but we did not find studies investigating the use of HDR images in FP description. Using uniformity, repeatability rate, mean average precision, and matching rate metrics, we compared the performance of the CP_HDR algorithms using LDR and HDR images. We observed an increase in the uniformity of the distribution of FPs among the high-light, mid-light, and low-light areas of the images. The results show that using HDR images as input to detection algorithms improves performance and that SfHDR and HfHDR enhance FP description.

Keywords—High Dynamic Range, HDR images, detection, description, feature points.

I. INTRODUCTION

Several computer vision applications, such as 3D reconstruction, face recognition, image stitching, and object tracking, rely on feature points (FPs) detection and description [1]–[4]. Most FP detection algorithms are designed for low dynamic range (LDR) images. When a scene has extreme light conditions (with very dark and bright areas), the FP detector performance decreases due to under and overexposed areas in the image, missing potential FPs. High dynamic range (HDR) images can be used to overcome these problems [5].

FP extraction algorithms detect and describe characteristics in images. The detection aims to find FPs in regions that represent image features. Good FP extraction algorithms detect FPs robust to image transformations such as rotation, point of view, and scale. The description involves assigning a description vector that identifies the detected FP. An ideal description allows

the identification of a certain FP even after several image transformations or different captures of the same scene [6], [7].

One of the major challenges in this area is to extract FPs from images with extreme lighting conditions, where low dynamic range (LDR) images can not accurately register and some areas of the image may end up being under or overexposed. The range of values that can be represented in an image is called dynamic range. While LDR image pixels usually can represent 2^8 tones per sample [8], HDR images are those whose pixels can represent more than 2^8 tones (generally, 2^{32} tones) per sample.

If the difference between a scene’s brightest and darkest regions is greater than its dynamic range, the brightest or darkest regions can be noisy, losing details. As HDR images have a greater dynamic range than LDR images, HDR can better represent scenes with extreme lighting conditions, especially in underexposed and overexposed areas [9].

Since FP extraction depends on the scene’s lighting, using HDR images in FPs extraction can increase the number of FPs detected in saturated regions in LDR images [5], [10]–[12]. Furthermore, employing descriptors that enable a reliable description of these points can improve the performance of applications that use FP description.

However, most FP extraction algorithms are designed to receive LDR images as input, and modifying the canonical algorithms to receive HDR images is a laborious task. Most studies that use HDR, use tone mapping (TM) algorithms to transform HDR into LDR images [5], [10], [11], [13], [14]. In previous studies, we have shown that using HDR images instead of LDR as input to FP extraction algorithms lead to better detection and description metrics [12], [15], [16].

In this study, we propose a library called CP_HDR that can receive both LDR and HDR images as input to detection and description algorithms. We use the CP_HDR library to compare the detection and description algorithms performance when using LDR and HDR images as input. The CP_HDR is designed to be easy-to-use and popularize the FP extraction with HDR images as input, providing both canonical and HDR-optimized FP extraction algorithm. We made a systematic review to understand the state-of-the-art and list the datasets, algorithms, and metrics that are being used in the literature (Section II); based on the systematic review results, we have implemented the CP_HDR library. The metrics, datasets, algorithms and execution pipeline implemented are described in Section III. Afterwards, we compared our implementation with previous

studies, showing the results (Section IV) and conclusions (Section V).

II. SYSTEMATIC REVIEW

This section describes a systematic review (SR) about FP detection and description algorithms using HDR images as input. The SR consists of three steps: *planning*, *conduction*, and *description*. In the planning step, the main objective and protocol are defined. In the conduction step, the studies are searched and selected. In the description step, the relevant information is extracted and described [17], [18].

A. Planning

The main objective of this SR is to find relevant studies that explore FP detection and description algorithms that use HDR images as input or detail how detection and description in HDR images are made, comparing the algorithms performance when using HDR and LDR images. With that in mind, we formulated four search questions (SQs). **SQ1**: Which are the tone mapping techniques used? **SQ2**: Which are the detection and description algorithms used? **SQ3**: Which are the evaluation metrics used? **SQ4**: Which are the datasets used?

To find peer-reviewed studies, we used the following search sources: IEEE Xplore, ACM Digital Library, Elsevier Scopus, Springer Link, and Web of Science. The search string used was: ('Keypoint' OR 'Feature Point' OR 'Feature detection') AND ('detection' OR 'detector' OR 'description' OR 'descriptor') AND ('High Dynamic Range' OR 'HDR') AND 'Image'. The search string slightly changed depending on the search source due to syntax differences.

Three inclusion criteria (IC) and five exclusion criteria (EC) were used to define if a study is selected or discarded. **IC1**: the study proposes an approach for detecting or describing FPs in HDR images. **IC2**: the study describes the development of an FP detection or description algorithm that receives an HDR image as input. **IC3**: the study compares FP detectors or descriptors using LDR and HDR images as input. **EC1**: the study is not in Portuguese or English languages. **EC2**: only the abstract is available. **EC3**: the study is not accessible. **EC4**: no inclusion criteria were detected. And **EC5**: is not a primary source (reviews, mappings, surveys, tutorials etc).

B. Conduction

The conduction step used the search string to find studies in the search sources. The duplicated and unavailable studies were discarded. Afterwards, the studies were read, and those who met any IC and no EC were selected to extract relevant information.

We found 259 studies in IEEE Xplore, 166 in Springer Link, 104 in Web of Science, 177 in ACM Digital Library, and 29 in Elsevier Scopus search source. After reading the studies, we identified that 67 were duplicated, and 640 fitted some exclusion criteria. Therefore, 21 studies were selected to extract information. Figure 1 shows the number of studies found and the number of studies selected for information extraction.

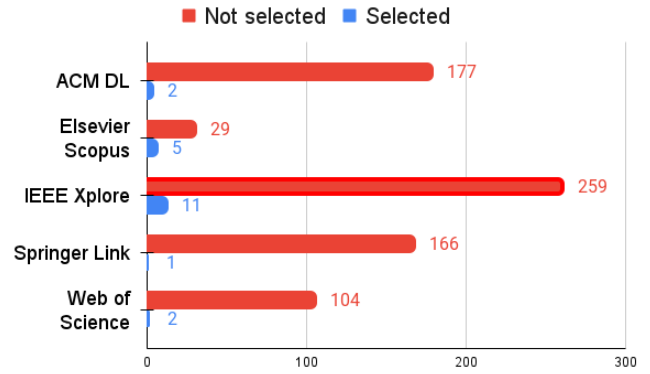


Fig. 1: Selected and not selected studies in each of the search sources.

C. Description

The last step of the SR consists of reading all the selected studies to verify if it has information that can be extracted to answer the SQs defined in the planning step. In this section, we describe the selected studies.

Chermak and Aouf (2012) [19] study detecting and matching FPs in scenes with high-light and low-light areas using HDR images. The authors use an LDR capture system and an HDR capture system to compare the effectiveness of using HDR images. Using the software FLANN to match FPs, the authors reported that the matching improved up to 29.35 times when using the HDR capture system.

Kontogianni et al. (2015) [20] evaluate FP detection in scenes containing buildings. The Mantiuk [21] TM algorithm is used to convert HDR images into LDR (TM-LDR images), and FPs are described using SIFT, SURF, FAST, and ORB. The authors observed that the ORB algorithm detected more FPs when using the TM-LDR images. ORB also performed faster when compared to the other descriptors used.

Jagadish and Sinzinger (2008) [22] use a detector focused on detecting junction points in the façade of buildings, i.e., corners and vertices [23]. A rotation invariant descriptor [24] and SIFT algorithm is used as the benchmark. The authors observed an increase of 19.35% in the matching and a 15% better sensitivity in the proposed approach compared to SIFT.

Zhuang and Liang (2019) [13] propose an approach for extracting locally invariant FPs. The authors developed two TMs: one based on the reflection of light in the scene (called *reflection layer*) and another based on the scene's lighting (called *illumination layer*). The FP detection uses the reflection layer, while the description uses the illumination layer. For FP detection, the authors used the FAST detector and the binary descriptor for description. With this approach, the authors report that there was an improvement in FP detection when compared to using HDR images. While the approach using HDR images detected 11 FPs, 990 FPs were detected using the proposed approach. In FP matching, using an HDR image resulted in 4

FPS matched, while when using the proposed approach, 139 were matched.

Ige et al. (2016) [25] used support vector machines (SVMs) and local binary pattern (LBP) for the facial expression recognition task. The proposed method receives image descriptions as input. For description, the authors used SURF with original LDR images and a TM-LDR image generated when applying a TM algorithm [21] to the HDR image. The authors reported that the TM-LDR image approach presented better results, reaching 79.8% accuracy. In contrast, the traditional methods—without using SVM, LBP, and using LDR images—obtained between 31.3 % and 70.8% accuracy.

Mukheerjee et al. [14] proposed a convolutional neural network (CNN) that receives an HDR image for object detection. They propose a methodology to generate and validate a large scale annotated HDR dataset from an existing LDR dataset, and create an out of distribution (OOD) HDR dataset to test and compare the performance of HDR and LDR trained detectors under extreme lighting conditions. To generate the HDR dataset, they use the Kovaleski et al. [26]; Huo et al. [27], Eilersten et al. [28], and Marnerides et al. [29] expansion operators (EOs) to expand LDR images into HDR. The FasterRCNN [30], SSD300 and SSD512 [31] detectors and PascalVOC 2007 [32], PascalVOC 2012 [33] and a personal dataset was used. Authors reported that using the proposed methodology, HDR trained models are able to achieve from 10 to 12% more accuracy compared to LDR trained models.

Due to their continuity, four groups of studies were organized by author and theme: Section II-C1 describes three works developed by Melo et al. and Nascimento et al.; Section II-C2 describes two studies developed by Přebyl et al.; Section II-C3 describes six studies developed by Rana et al.; and Section II-C4 describes studies focused on tracking and localization.

1) Melo et al. and Nascimento et al. studies:

Melo et al. (2018) [12] describe an approach using HDR images as input to detection algorithms. The SIFT Difference of Gaussian (DoG) detector and the Harris corner detector are modified to support HDR images by adding one more step in the detection with the application of a local mask based on the coefficient of variation (CV). In Harris corner, the CV mask is applied after the Gaussian filter, while in DoG, the CV mask is applied to all images of the scale space. The 2D and 3D lighting datasets from Přebyl et al. (2012) [10] were used for testing. A significant improvement was obtained in the uniformity rate metric when using HDR images compared to their LDR versions.

Nascimento et al. (2022) [15] adapted the canonical SIFT algorithm to receive HDR images and compared the description performance from the algorithms when using LDR and HDR images. Using mAP metric, 2D lighting and 3D lighting datasets from Přebyl et al. [10], results show that using HDR images increase mAP by 61.50% in 2D lighting and 81.80% in 3D lighting dataset.

Nascimento et al. (2023) [16] proposes a new detector, based on coefficient of variation (CV) and designed for HDR images, called DetectorCV. The DetectorCV is compared with Harris [34], DoG [35], SURF [36], Harris for HDR, DoG for HDR and SURF for HDR [12] detectors, using Uniformity [12]

and RR metrics, with ProjectRoom dataset from Rana et al. [5], 2D lighting and 3D lighting datasets from Přebyl et al. [10]. Results show that DetectorCV outperforms other detectors in Uniformity metric. The DetectorCV outperforms Harris, DoG, DoG for HDR and SURF for HDR algorithms in RR metric.

2) Přebyl et al. studies:

Přebyl et al. (2012) [10] investigates if HDR imagery improves FP detection performance when compared to LDR images. The authors have elaborated a dataset¹ with equivalent scene captures in LDR and HDR images. The scenes were captured in LDR format, with 10 different exposure times. Then, Debevec algorithm [37] was used to generate HDR captures. The dataset consists of two scenes: a planar (2D) scene containing three posters in A4 sheets next to each other, attached to a box; and a 3D scene containing several non-planar rigid objects. Each scene is captured in three different sequences:

- **Viewpoint:** the scene is captured 21 times in a circular trajectory around the scene's center with a step of 2.5 degrees, resulting in a viewpoint range of 50 degrees.
- **Distance:** the scene is captured seven times, and the distance between the camera and the scene increases exponentially, yielding the distance sequence of 100, 103, 109, 122, 147, 197, and 297 cm.
- **Lighting:** the scene is captured seven times, each time with different combinations of 3 light sources being on or off, with at least one on.

The authors used a \log_2 transformation as global tone mapping (GTM) and Zuiderveld [38] algorithm as local tone mapping (LTM) to transform the HDR images into new tone-mapped LDR versions of the captures. The authors added preprocessed LDR images using Wallis-Filter [39] (WAL) to equalize contrast. Figure 2 shows examples of the capture sequences from Přebyl et al. (2012) dataset [10].

Přebyl et al. (2012) [10] compared Harris corner [34], Shi-Tomasi [40], FAST [41] and SURF [36] detectors performance using the LDR and tone-mapped LDR (TM-LDR) versions of the captures. As a result, they found that the approaches using GTM and LTM resulted in a higher repeatability rate (RR) than the others. They also observed that, on average, the 2D dataset had a lower RR than the 3D dataset.

Přebyl et al. (2016) [11] used several TM algorithms to transform HDR into LDR images, used the resulting TM-LDR images as input to FP detection algorithms, and compared the FP detection when using the different TM-LDR images. Using the dataset elaborated in their previous study [10], they generated six different versions of the captures using global TMs, five using local TMs, one LDR capture, one LDR preprocessed version using canonical histogram equalization, one LDR preprocessed version using CLAHE histogram equalization [42], one version using a linear mapping from HDR to LDR, and one version using a logarithmic mapping from HDR to LDR. They used Harris corner [34], Shi-Tomasi [40], FAST [41], SURF [36] and SIFT (DoG) [35] as detectors.

¹Dataset by Přebyl et al. [10], available at: http://www.fit.vutbr.cz/~ipribyl/FPinHDR/dataset_JVCI. (Accessed on July 01, 2023).

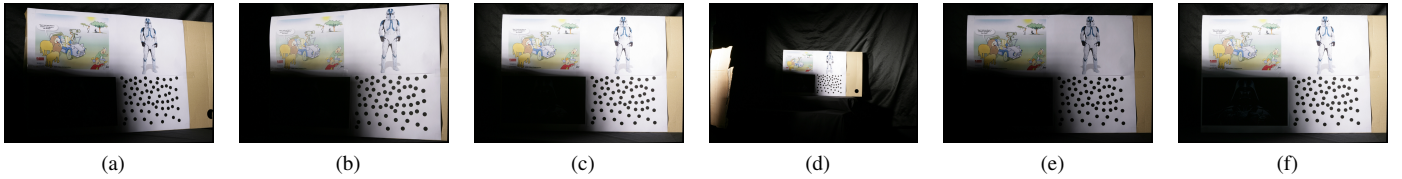


Fig. 2: Capture sequences examples from Pribyl et al. (2012) [10] 2D dataset. (a) and (b) from viewpoint capture sequence, (c) and (d) from distance capture sequence, and (e) and (f) from illumination capture sequence.

Pribyl et al. (2016) [11] observed that global TMs have the side effect of compressing the contrast of the intermediate tones of the image since they take into account the global illumination. The values of the very light and very dark areas have greater weight than the intermediate values. Among the TMs used, Reinhard et al. [43] present the worst performance, detecting few FPs. The FAST detector presented poor performance when used with global TMs, being sensitive to contrast compression.

On the other hand, when using local TM, more FPs were detected compared to when global TMs were used. Even so, detection in dark areas proved difficult, given that few or no FPs were detected. When using Fattal [44] and Mantiuk [21] TM algorithms, a higher number of FPs were detected when compared to other TM algorithms [11].

3) Rana et al. studies:

Rana et al. investigates the use TM algorithms to convert HDR into LDR images and use the TM-LDR images as input to detection and description algorithms. First, Rana et al. [5] elaborated a dataset² of two scenes: ProjectRoom (PR) and LightRoom (LR). The PR scene comprises eight different lighting configurations created by blocking a subset of the light sources. The LR dataset comprises seven different natural lighting conditions obtained by changing how closed the room blinds are and the position of a tungsten lamp [5]. Similarly to Pribyl et al. [10], Rana captured the dataset using LDR techniques and generated the HDR images using Debevec algorithm [37]. Figure 3 shows examples of captures from Rana et al. [5] dataset.

In addition to the dataset, Rana et al. (2015) [5] explored TM algorithms and used TM-LDR images as input to FP detection algorithms. The authors used different TMs than previous studies [10], [11]. They used two global TMs, seven local TMs, linear mapping, logarithmic mapping, perceptually-uniform mapping [45] (PU-HDR), with the 2D illumination and 3D illumination datasets from Pribyl et al. (2012) [10]. When using SURF and Harris corner detectors, the authors observed that all approaches using TM images as input resulted in a better RR than when using LDR. The PU-HDR TM method showed better RR than global and local TMs.

Rana et al. (2016a) [46] studied the use of TM-LDR images to improve the performance of FP description algorithms. The authors used image matching, mean average precision (mAP),



Fig. 3: Capture examples from Rana et al. (2015) [5] dataset. (a), (b) and (c) from ProjectRoom scene, and (d), (e), and (f) from LightRoom scene.

and mean repeatability rate (mRR) as performance metrics. SIFT [35], SURF [36], FREAK [47], and BRISK [48] were used as description algorithms. The input images used were one LDR, two TM-LDR using global TMs, five TM-LDR using local TMs, one using a logarithmic mapping from HDR to LDR, and one linear mapping from HDR to LDR. The authors observed that the worst results were obtained using linear mapping images, while TM-LDR images presented better RR and mAP values. All TM-LDR techniques performed well with description algorithms, with marginal gains for SIFT.

Rana et al. (2016b) [49] investigated the optimization of retinex-based models using correlation coefficient (CC) and repeatability rate (RR) of reflectance images obtained from two retinex-based TMs: bilateral tone mapping operator (BTMO) and Gaussian tone mapping operator (GTMO). Four algorithms were created: BTMO optimized with CC (CCBTM), BTMO optimized with RR (RRBTM), GTMO optimized with CC (CCGTM), and GTMO optimized with RR (RRGTM). Shi-Tomasi [40] and Harris corner [34] were used as detection algorithms. In addition to the TM algorithms created, other

²Dataset by Rana et al. [5], available at: <http://webpages.l2s.centralesupelec.fr/perso/giuseppe.valenzise/sw/HDR%20Scenes.zip>. (Accessed on July 01, 2023).

local and global TM algorithms were used for comparison. The RR and CC metrics improved when using CCBTM, RRBTM, CCGTM, and RRGTM. The RRBTM and RRGTM detected more FPs [49].

Rana et al. (2017a) [50] developed the learning-based adaptive tone mapping operator (AdTMO), a framework to enhance FP detection stability under drastic illumination variations. The AdTMO is modulated based on a support vector regression (SVR) model using local higher-order characteristics. To compare with AdTMO, the authors used the GTMO, BTMO [49], Chiu [51], Drago [52], Reinhard [43], and Mantiuk [21] TM algorithms. The Harris corner [34], Shi-Tomasi [40], FAST [41], SURF [36], and SIFT [35] were used as detectors. The authors showed that the AdTMO presents a significantly better RR metric in all cases, with rates between 10% and 45% higher than the second best operator (BTMO) [50].

Rana et al. (2017b) [53] developed the learning-based descriptor-optimal tone mapping operator (DesTMO), a framework to tone-map HDR content for image matching under drastic illumination variations. A luminance invariant guidance model using an SVR to adapt the tone mapping function for image matching in scenes subject to a wide variety of illumination changes was used. The authors observed that DesTMO had significantly better rates of correct FP matches and mAP than the other TMs used in the comparison [53].

Finally, Rana et al. (2019) [54] developed a two-step framework, called (OpTMO), composed of a luminance-invariant guidance model based on an SVR to optimally adapt the tone mapping function for image matching and an energy maximization model to generate appropriate training samples for learning the SVR. At each step, the framework collectively addresses both FP detection and description steps in the feature matching. OpTMO is compared with some conventional TMs, AdTMO [49], and DesTMO [53]. The experimental results show that OpTMO is equivalent to DesTMO in FPs detection, presenting similar repeatability. As for its use in image matching, OpTMO presented better RR than all the others TMs, with rates between 10% and 53% better than the second best-placed, DesTMO [54].

4) Tracking and localization studies:

Yeh et al. (2021) [55] evaluates the use of HDR-based images to run an RGB-D SLAM [56] framework. The authors used a deep learning model that takes an LDR image as input and generates an HDR image, that is used to generate a radiance map which is normalized. An ORB descriptor is trained to receive normalized radiance maps and generate its description. The dataset TUM RGB-D [57] and a private dataset are used to evaluate the deep learning model. Yeh et al. (2021) used image matching as metric, comparing the results obtained using the ORB-SLAM2 [58] algorithm, the proposed framework with normalized radiance map, and the proposed framework with radiance map not normalized to verify if the radiance map normalization influences the image matching. The authors observed that the framework using the normalized radiance map presented a higher mean detection than the other approaches.

Albrecht et al. (2019) [59] evaluated the usage of TM algorithms to transform HDR into LDR images and use the resulting TM-LDR images as input to the ORB-SLAM2

algorithm. The HDR images were generated using Mertens et al. [60] algorithm. With HDR images, some TMs were applied and used as input to an ORB-SLAM2 algorithm. The authors observed that using TM-LDR images brought benefits in complex lighting scenes. However, the tracking algorithm fails in critical situations such as lighting transition (leaving a dimly lit room to an open sunny environment, for example).

Chermak et al. (2014) [3] used LDR and HDR images as input to the Kanade–Lucas–Tomasi (KLT) tracking algorithm, as implemented in OpenCV. An LDR capture system and an HDR capture system were used with SIFT [35], SURF [36], GFTT [40] and FAST [41] algorithms. The authors observed that the approach using HDR images showed results up to 29.35 times better when compared to those using LDR images.

Jinno et al. (2013) [61] developed a TM algorithm specialized in security systems that capture HDR images to improve object tracking in the scene. The authors modified the SIFT in order to optimize the processing time. The modification consists of using a mask to remove the image’s background, reducing the area to be processed. The authors observed that, compared to other TMs, the developed method significantly improves object tracking.

5) Systematic review conclusions:

Using HDR images as input to detector and descriptor algorithms requires changing these algorithms to support the dynamic range of HDR images correctly. Because of this necessity, most studies use a TM algorithm to enhance the image and get better results in detection and description. Some studies have proposed new TMs to improve specific tasks, such as invariance to environment illumination [53] or object tracking in security cameras [61].

Mantiuk, Reinhard, Drago, and Fattal were the most frequently used TM algorithms, with respectively 9, 8, 6, and 6 studies using them. The most used FP extraction algorithms are SURF [36] (11 studies), SIFT [35] (10 studies), Harris [34] (8 studies), and FAST (8 studies).

Yeh et al. [55] used an HDR image to calculate a normalized radiance map and used it as input to their proposed framework. On the other hand, only Melo et al. (2018) [12] and Nascimento et al. (2022) [15] used HDR images as input to detection and description algorithms. Furthermore, only two studies proposed and made their datasets available [5], [10].

Table I lists the TM methods, the detectors, the descriptors, the evaluation metrics, and the datasets used in each study.

III. METHODS

In this study, we propose a library called CP_HDR, capable of detection and description using LDR or HDR images as input. We compared the results obtained using LDR and HDR images. The library has state-of-the-art metrics (Section III-A), well-known detector and description algorithms with support to LDR and HDR images, modifications to improve detection and description in HDR images (Section III-A5), and an automatic script to generate the intensity segmentation (Section III-B). The experiment pipeline is explained in Section III-C.

TABLE I: Systematic review summary.

	Use HDR?	TM algorithms	Detector	Detector metrics	Descriptor	Descriptor metrics	Used dataset
Přibyl et al. (2012) [10]	-	[38]	Harris Corner, GFTT, FAST, SURF	RR	-	-	[10]
Chermak et al. (2012) [19]	Yes	-	SIFT, Harris, GFTT, SURF, FAST	-	SIFT, SURF	FLANN accuracy	personal, not available
Jinno et al. (2013) [61]	-	[62], [63]	Modified SIFT	-	Modified SIFT	Tracking accuracy	personal, not available
Chermak et al.(2014) [3]	Yes	-	SIFT, SURF, GFTT, FAST	Amount of FPs	KLT (tracking)	tracking performance	personal, not available
Rana et al. (2015) [5]	-	[51], [52], [44], [64], [65], [21], [66], [62], [67]	Harris, SURF	mRR	-	-	[5]
Kontogianni et al. (2015) [20]	-	[21]	SIFT, SURF, FAST and ORB	Amount of detected FPs and processing time	-	-	personal, not available
Přibyl et al. (2016) [11]	-	[21], [64], [62], [43], [68], [44], [69], [70], [71]	Harris, GFTT, SIFT, SURF, FAST, BRISK	mRR	-	-	[10]
Ige et al. (2016) [25]	-	[21]	LBP	-	SURF	Face recognition accuracy	personal, not available
Rana et al. (2016a) [46]	-	[62], [52], [21], [44], [51], [72]	SIFT, SURF, FREAK, BRISK	mRR	SIFT, SURF, FREAK, BRISK	mAP	[5]
Rana et al. (2016b) [49]	-	[21], [62], [51], [72], [52]	Harris and SURF	RR and CC	-	-	[5]
Rana et al. (2017a) [50]	-	[62], [21], [49], [52], [51], [72]	Harris, GFTT, FAST, BRISK, SURF and SIFT	RR	-	-	[5]
Rana et al. (2017b) [53]	-	[62], [21], [51], [49], [52]	SURF, SIFT, FREAK, BRISK	-	SURF, SIFT, FREAK, BRISK	mAP and matching score	[5]
Jagadish et al. (2018) [22]	-	[44]	[23]	-	[23]	Amount	personal, not available
Melo et al. (2018) [12]	Yes	[44], [21]	Harris, SIFT	mRR, uniformity rate	-	-	[10], [5]
Zhuang et al. (2019) [13]	Yes	-	BRISK	Amount of FPs	BRISK	amount of matched FPs	personal, not available
Albrecht et al. (2019) [59]	-	[72], [21], [52], [9]	ORB	-	ORB	Analysys with SLAM	personal, not available
Rana et al. (2019) [54]	-	[52], [51], [72], [62], [73], [74], [75]	Harris, BRISK, FREAK, FAST, SURF and SIFT	RR	BRISK, FREAK, SURF and SIFT	mAP	[5]
Yeh et al. (2021) [55]	Yes	-	ORB	average detection	ORB	average matching	personal, not available and TUM RGB-D
Mukherjee et al. (2021) [14]	Yes	[26], [27], [28], [29],	FasterRCNN [30], SSD300 and SSD512 [31]	-	ORB	mAP	personal, not available [32], and [33]
Nascimento et al. (2022) [15]	Yes	-	DoG	-	SIFT	mAP	[10], [5]
Nascimento et al. (2023) [16]	Yes	-	Harris, DoG, SURF, DetectorCV, Harris for HDR, SIFT for HDR, SURF for HDR	RR, Uniformity	-	-	[10], [5]

A. Metrics

As seen in Section II-C5, repeatability rate (RR) is the most used metric to evaluate FP detection. In the FP description, matching score and average precision (AP) are the most used metrics. Melo et al. [12] proposed the uniformity rate (UR) as an FP detection metric to verify whether an algorithm detects FPs in areas of the image with extreme lighting conditions. This metric is specially suitable to the purpose of this study, as we are comparing LDR and HDR detection and description algorithms. HDR images have a greater dynamic range than LDR images, so the UR can be used to verify how this feature influences the detection results in image areas with low or high luminosity.

1) Repeatability rate (RR):

The RR metric indicates the percentage of FPs in a reference image (I_r) that are detected in a test image (I_t). The RR evaluates the stability of the detector between captures of the same scene, resulting in a value in the interval $[0.0, 1.0]$. Values closer to 1 indicate that more FPs were detected in the two images.

Let n_r and n_t be the total of FPs found in I_r and I_t respectively. Let M be the maximum number of FPs considered in the analysis, and let R_{rt} be the number of FPs found in both I_r and I_t . The RR between I_r and I_t is defined by

$$\text{RR}(I_r, I_t) = \frac{R_{rt}}{\min(n_r, n_t, M)} \quad (1)$$

When there is no reference image but several captures of the same scene, we can use the summarized repeatability rate (sRR) as follows: we calculate the RR for all permutations between the captures of the scene and calculate the results average. All possible non-ordered pairs of different images are considered. Let n be a number of captures in a given dataset. The sRR is defined by

$$\text{sRR} = \frac{\sum_{i=1}^{n-1} \sum_{j=i+1}^n \text{RR}(i, j)}{\sum_{k=1}^{n-1} k} \quad (2)$$

2) *Uniformity rate (UR)*: The UR is a metric to measure the quality of FP detection in areas of the image with different luminosities [12]. In this study, we use the UR to evaluate how well the algorithms detect FPs in brightest, intermediate, and darkest areas of the image. We made an intensity segmentation of the image pixels, as detailed in Section III-B. The value returned by the UR is in the interval $[0.0, 1.0]$, where the best result is 1.0. The best result means that the FPs are equally distributed among groups of pixels with different illumination levels in the image.

Let T be the total number of detected FPs, let n be the number of pre-divided groups of the image, and let a_i be the number of FPs detected in the i -th group of the image. The UR is defined by

$$U = 1 - \left(\max_{1 \leq i \leq n} \left(\frac{a_i}{T} \right) - \min_{1 \leq i \leq n} \left(\frac{a_i}{T} \right) \right) \quad (3)$$

3) Matching:

To match FPs, we use the nearest neighbor distance ratio (NNDR) [76]. This quotient is often used to evaluate matching between two FPs [2]. NNDR calculates the distance from the description vector to its nearest neighbor and its second nearest neighbor.

Let d_1 and d_2 be the distances to the nearest neighbor and the second nearest neighbor respectively. Let D_t be the target description vector. Let D_1 and D_2 be the description vectors of the two nearest neighbors of D_t . NNDR is defined by

$$\text{NNDR} = \frac{d_1}{d_2} = \frac{\|D_t - D_1\|}{\|D_t - D_2\|} < \text{th} \quad (4)$$

The matching between two description vectors is considered as true positive (tp) if the NNDR value is less than a defined threshold (th) and false positive (fp) otherwise. We used 0.7 as the threshold value and the Euclidean distance to calculate the distance between two description vectors [15].

4) Mean average precision (mAP):

The average precision (AP) metric evaluates matching between FPs obtained from two captures of the same scene. The AP can be obtained by calculating the area under the ROC curve [46], [76]. To calculate the ROC curve, we need the values of precision (Equation 5) and recall (Equation 6), where tp, fp, and fn are, respectively, the number of true positives, false positives, and false negatives.

$$P = \frac{\text{tp}}{\text{tp} + \text{fp}} \quad (5)$$

$$R = \frac{\text{tp}}{\text{tp} + \text{fn}} \quad (6)$$

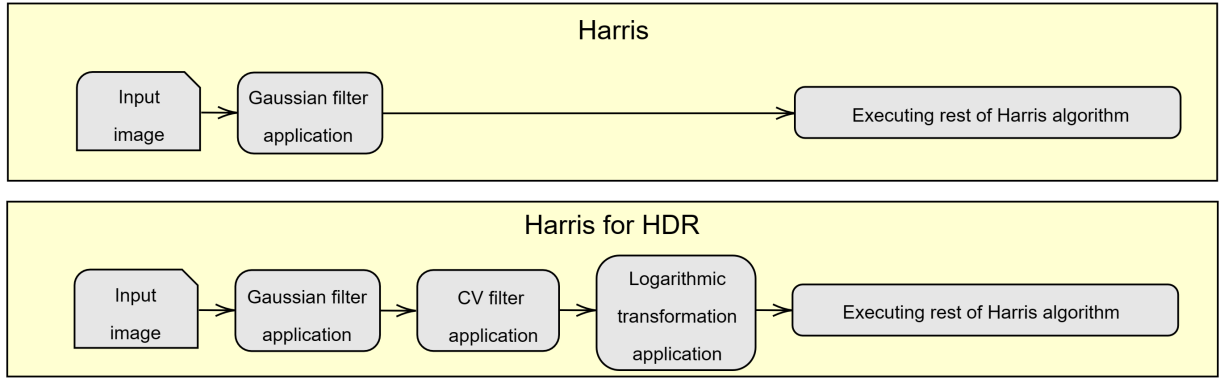
The ROC curve is obtained by calculating the precision and recall values for a sequence of th values from the NNDR. The average APs for all permutations of image pairs in a dataset is called mean average precision (mAP).

5) Algorithms and modifications:

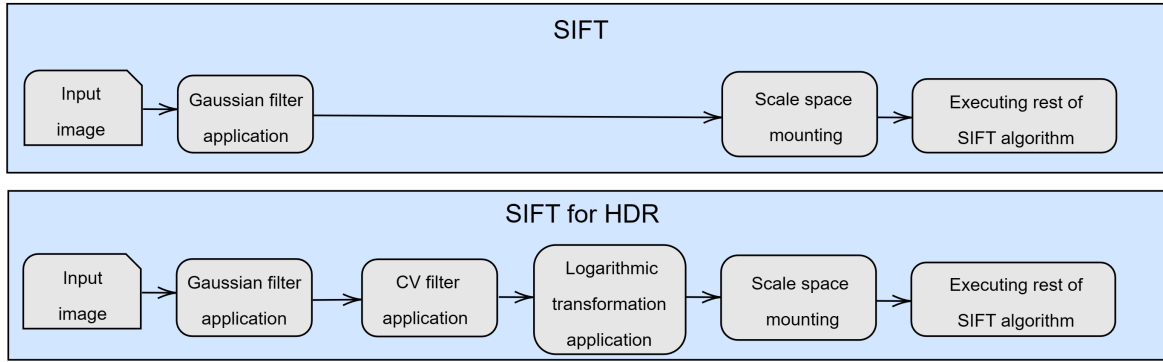
The modification in Harris corner and DoG proposed by Melo et al. [12] consists in adding a coefficient of variation (CV) filter in an intermediate step of the detection algorithm. The CV is defined as the ratio of the standard deviation (σ) to the arithmetic mean (μ) of a given population, e.g., a set of pixels. Considering a population of n elements, Equation 7 calculates the CV [77]. Figure 5 shows an example of the CV filter application on LDR and HDR images.

$$\text{CV} = \frac{\sigma}{\mu} = \frac{\sqrt{\frac{1}{n} \sum_{i=1}^n (x_i - \mu)^2}}{\frac{1}{n} \sum_{i=1}^n x_i} \quad (7)$$

The coefficient of variation filter is used as an intermediate step in the HfHDR and SfHDR detectors to improve FP detection in darker image areas. In the HfHDR, the CV mask is applied to the input image after the Gaussian filter application step. After applying the CV filter, a logarithmic transformation is applied to the resulting image, and then algorithm continues as in the original Harris corner algorithm. In the SfHDR detector, a CV filter is applied to the input image followed by



(a)



(b)

Fig. 4: Modification of the canonical detectors to implement the (a) Harris for HDR and (b) SIFT for HDR.

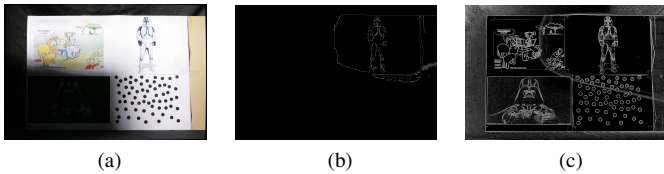


Fig. 5: Example of CV filter application on images: (a) reference image; (b) CV filter applied on a LDR capture; and (c) CV filter applied in a HDR capture.

a logarithmic transformation before creating the scale space. Afterwards, the algorithm continues as in the original version by building the scale space. Figure 4 illustrates where Harris and SIFT algorithms were modified. For further details regarding the implementations of the CV filter and the logarithmic transformation, please refer to Melo et al. (2018) [12].

B. Datasets

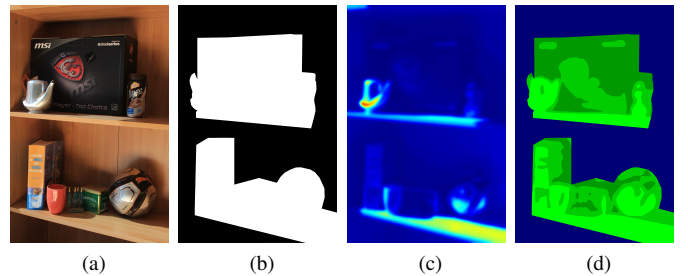


Fig. 6: Intensity segmentation example of DR dataset: (a) reference image; (b) the ROI mask that separates the background from the foreground; (c) the luminance map generated using the original image and rendered as a heat map; and (d) the final segmentation of the image's foreground.

Two datasets were created to explore extreme light conditions in scenes with LDR and HDR images. Přibyl et al. [10] dataset (DP) was detailed in Section II-C2 and Rana et al. [5] dataset (DR) was detailed in Section II-C3. Both datasets were used

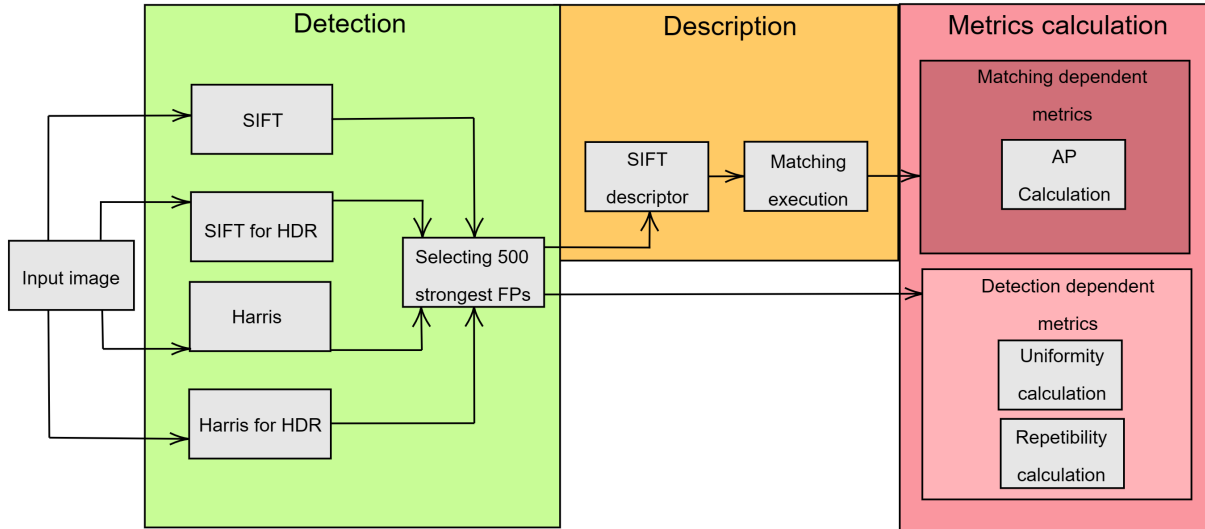


Fig. 7: Execution pipeline. The green area refers to the FP detection, while the orange area refers to the description step. The red area refers to the metrics calculation step.

in several other studies [5], [10]–[12], [15], [16], [46], [49], [50], [53], [54]. In this study, we used the DR dataset and the three 2D capture sequences from DP dataset [10].

1) *Dataset intensity segmentation*: The UR metric requires the segmentation of the image areas with different lighting intensities. The DP dataset provides ROIs to the image areas with high, medium, and low lighting, but the DP dataset does not provide it. We have implemented the following approach that segment an image in groups of lighting intensities, and can be used to segment any dataset scene. We used an approach similar to Nascimento et al. (2023) [16], described below.

First, we manually created a ROI to separate the background area from the foreground in the captures. The background is an area of the image with no features and where FPs are not usually detected. Each pixel in the foreground was assigned to one of three groups of lighting intensity: brightest, intermediate, and darkest pixels. We generated a luminance map for each capture to segment the image into the three groups. Then, we used the luminance map to select the brightest one-third of pixels, the intermediate one-third of pixels, and the darkest one-third of pixels. It resulted in three groups with a very similar amount of pixels, required for the UR metric.

To generate the luminance map, a Retinex algorithm was used. According to the Retinex theory, an image I is the product of the luminance L of the scene and the reflectance R . That is, $I = RL$ [49]. To find the luminance, we use the approach used by Chiu et al [51]. The luminance is defined as $L = I * G_r$, and G_r is a Gaussian filter with standard deviation calculated based on the image size $m \times n$, in the form: $r = \alpha \max(m, n)$. The α constant used was 0.007, and the Gaussian mask size used was the smallest odd number greater than $6r$, as in previous studies [15], [16], [49].

A cumulative histogram H was calculated considering only

the foreground in the luminance map. After that, we defined a threshold to divide the foreground into three groups, each one with approximately one-third of the pixels of the foreground. Figure 6d shows an example of segmentation of the original image, with the background in blue, the darkest group of the image in dark green, the group with the intermediate incidence of illumination in medium green, and the brightest group of the image in light green.

Figure 6 shows an example of the steps to segment an image. Figure 6a shows the original image, while Figure 6b shows the ROI mask created manually to separate the foreground from the background. Figure 6c shows the luminance map rendered as a heat map.

C. Pipeline execution

To run the experiments, we used Rana et al. intensity segmented dataset. The Příbyl et al. dataset already provides intensity segmentation. We used the FPs generated by Harris and Harris for HDR with SIFT descriptor to create the Harris+SIFT and HfHDR+SIFT descriptors.

We run the detection algorithms. Then, we classify all detected FPs based on their response to the detector. The 500 FPs with the strongest response were selected, as done in other studies [5], [12]. The selected FPs were described using SIFT descriptor. For each dataset, we matched the FPs all possible pairs of distinct images and calculated the metrics.

The UR, RR, AP, mAP, and matching rates were calculated for Harris, Harris for HDR, SIFT, SIFT for HDR, Harris+SIFT, and HfHDR+SIFT algorithms. Figure 7 illustrates the execution flow of the experiments. As mAP and matching rate metrics are calculated after the execution of the experiments, they are not present in the illustration.

IV. RESULTS

Tables II to V show the metric values obtained for each dataset, where 2D distance, 2D lighting, and 2D viewpoint are from Přebyl et al. [10] dataset, and the ProjectRoom and LightRoom are from Rana et al. dataset [5].

A. Detection evaluation

Table II shows the results obtained with sRR and UR mean for each dataset used in this study. The best result is highlighted.

The Harris and SIFT algorithms presented better sRR values, but the HfHDR and SfHDR presented better UR values. SfHDR showed better UR values in three out of the five datasets. In most cases, the UR metric has better values when using HDR images. Figure 8 shows an example of FP detection using the LightRoom dataset and HfHDR algorithm. There, we can observe the improvement in the FP distribution when using HDR images, especially in darker and intermediate areas.

B. Description evaluation

Table III shows the mAP and the mean matching rate for each dataset used in this study. The best result is highlighted.

Both mAP and matching rate presented similar results in each database. The Harris+SIFT and HfHDR+SIFT algorithms showed better results than SIFT and SfHDR. The SIFT algorithm performs better when using 2D distance dataset, probably due to SIFT's scale-invariance. In almost all cases, the best results were obtained using HDR images. Overall, the HfHDR+SIFT algorithm showed improvement in the description when compared to Harris+SIFT, and the SfHDR showed a worse description when compared to SIFT.

While Přebyl et al. datasets contain images of a poster, Rana et al. datasets consist of scenes composed of several rigid objects positioned in such a way as to create shadows on other objects. In all metrics, when using the Rana datasets, the best results were obtained with the Harris or HfHDR algorithms. This may indicate that, in scenes with more complex lighting or geometry, corner detectors have an advantage over blob detectors.

The use of the CV filter and the logarithmic transformation in HDR images generate noise in the darkest regions and on the specular surfaces. But, when the CV filter is applied to LDR images, the resulting image showed edges only in the brightest regions of the image. Considering that the ProjectRoom dataset presented noisiest foreground when using HDR images and SfHDR and HfHDR+SIFT descriptors, we assume that this is why the best results in the ProjectRoom are obtained when using LDR images.

Figure 9 shows the FP matching using SfHDR algorithm. When HDR images are used, there are FP matches in the darkest area, while when using LDR images, there are no matches. Consequently, matching distribution between areas is improved when using HDR images. The UR metric confirms this, since most of the best URs were obtained when using SfHDR and HfHDR algorithms with HDR images.

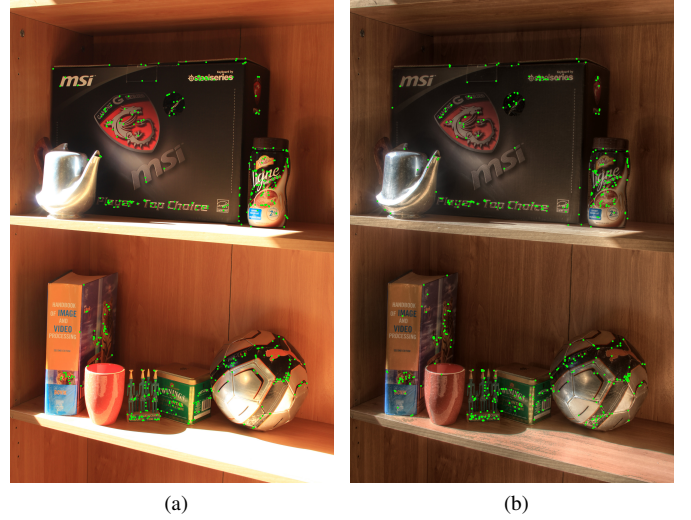


Fig. 8: FP detection using LightRoom dataset and HfHDR detector. (a) using LDR image and (b) using HDR image. For display purposes, HDR image was tone-mapped to LDR.

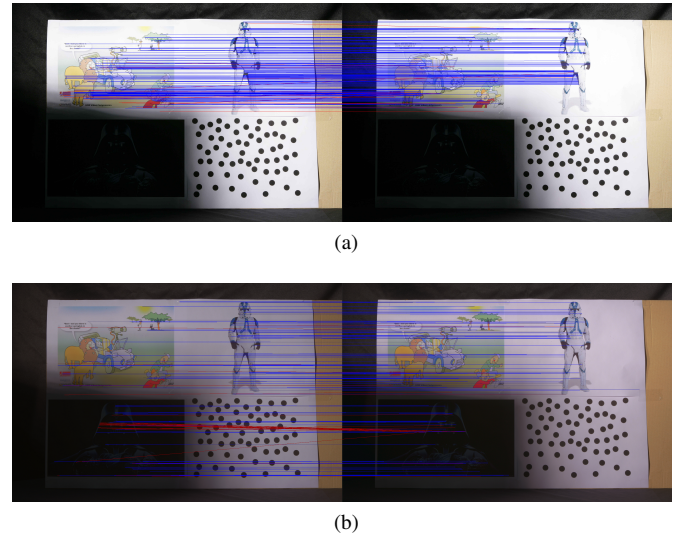


Fig. 9: Matching using SfHDR descriptions. Blue lines are correct matches, while red lines are incorrect matches. (a) using LDR image and (b) using HDR image.

C. Comparison with previous studies

Tables IV and V compare Melo et al. [12] results with ours, using sRR and UR metrics in the 2D distance, 2D lighting, and 2D viewpoint datasets. It is important to note that SIFT and SfHDR detector algorithms were significantly improved, with subpixel precision and code rewriting to fix several problems of code cohesion and minor bug fixes. This can explain the difference between results.

TABLE II: UR and sRR values using Harris, HfHDR, SIFT and SfHDR detectors for all datasets. The best results for each dataset are highlighted.

	Detector	Harris		HfHDR		SIFT		SfHDR	
	Database dynamic range	LDR	HDR	LDR	HDR	LDR	HDR	LDR	HDR
Mean repeatability (sRR)	2D distance	0,35581	0,17330	0,03914	0,15857	0,20143	0,26066	0,15981	0,07161
	2D lighting	0,02041	0,47553	0,00990	0,01161	0,04101	0,01314	0,01552	0,00981
	2D viewpoint	0,05168	0,05789	0,02087	0,02495	0,14597	0,04487	0,03022	0,01519
	LightRoom	0,41011	0,32425	0,05961	0,24409	0,16264	0,34942	0,04981	0,22219
	ProjectRoom	0,27704	0,25020	0,12238	0,07990	0,12734	0,13466	0,02000	0,07209
Mean uniformity (UR)	2D distance	0,28204	0,35080	0,08776	0,64780	0,24148	0,43342	0,35257	0,83200
	2D lighting	0,27465	0,15568	0,24440	0,72771	0,16073	0,36771	0,29542	0,78000
	2D viewpoint	0,24951	0,23182	0,05559	0,76610	0,14800	0,45657	0,35285	0,83285
	LightRoom	0,40260	0,10505	0,54991	0,83878	0,20640	0,19238	0,21314	0,68348
	ProjectRoom	0,58157	0,17471	0,81046	0,77689	0,68581	0,37095	0,65569	0,72779

TABLE III: Mean average precision (mAP) and matching rate values using Harris+SIFT, HfHDR+SIFT, SIFT and SfHDR descriptors for all datasets. The best result for each dataset is highlighted.

	Descriptor	Harris+SIFT		HfHDR+SIFT		SIFT		SfHDR	
	Database dynamic range	LDR	HDR	LDR	HDR	LDR	HDR	LDR	HDR
Mean average precision (mAP)	2D distance	0,68872	0,39798	0,29657	0,75337	0,44677	0,82056	0,45285	0,51048
	2D lighting	0,32830	0,35886	0,13837	0,31867	0,21669	0,33776	0,27214	0,23069
	2D viewpoint	0,45687	0,16820	0,00515	0,51096	0,46316	0,46357	0,43244	0,38100
	LightRoom	0,50288	0,35428	0,23895	0,55231	0,16552	0,49372	0,11931	0,46522
	ProjectRoom	0,66438	0,32320	0,27934	0,37020	0,30082	0,28835	0,11896	0,28746
Matching rate	2D distance	0,96028	0,53647	0,42108	0,91779	0,67077	0,98200	0,66566	0,69631
	2D lighting	0,47318	0,50426	0,20420	0,44893	0,32642	0,49055	0,40935	0,36054
	2D viewpoint	0,73680	0,27323	0,00896	0,82050	0,78493	0,74640	0,71270	0,63074
	LightRoom	0,63017	0,48615	0,31616	0,70434	0,22440	0,69950	0,16511	0,65916
	ProjectRoom	0,76277	0,37288	0,33243	0,40658	0,40326	0,36927	0,16329	0,39886

TABLE IV: Comparison between Melo et al. and this study using Harris and HfHDR detectors. The best result for each dataset is highlighted.

	Detector	Harris		HfHDR		Harris		HfHDR	
	Database dynamic range	LDR	HDR	LDR	HDR	LDR	HDR	LDR	HDR
Mean repeatability (sRR)	2D distance	0,64000	0,00000	0,00000	0,37000	0,01835	0,45263	0,00866	0,01009
	2D lighting	0,70000	0,00000	0,00000	0,43000	0,33066	0,17308	0,03638	0,14304
	2D viewpoint	0,00000	0,00000	0,00000	0,49000	0,04614	0,05324	0,01822	0,02180
Mean uniformity rate (UR)	2D distance	0,27000	0,39000	0,06000	0,42000	0,28204	0,35080	0,08776	0,64780
	2D lighting	0,35000	0,31000	0,22000	0,47000	0,27465	0,15568	0,24440	0,72771
	2D viewpoint	0,31000	0,38000	0,00000	0,41000	0,24951	0,23182	0,05559	0,76610
Melo et al.						CP_HDR			

TABLE V: Comparison between Melo et al. and this study using SIFT and SfHDR detectors. The best result for each dataset is highlighted.

	Detector	SIFT		SfHDR		SIFT		SfHDR	
	Database dynamic range	LDR	HDR	LDR	HDR	LDR	HDR	LDR	HDR
Mean repeatability (sRR)	2D distance	0,00000	0,00000	0,00000	0,25000	0,20143	0,26066	0,15981	0,07161
	2D lighting	0,00000	0,00000	0,00000	0,34000	0,04101	0,01314	0,01552	0,00981
	2D viewpoint	0,00000	0,00000	0,00000	0,29000	0,14597	0,04487	0,03022	0,01519
Mean uniformity rate (UR)	2D distance	0,28000	0,43000	0,02000	0,62000	0,24148	0,43342	0,35257	0,83200
	2D lighting	0,25000	0,29000	0,13000	0,64000	0,16073	0,36771	0,29542	0,78000
	2D viewpoint	0,29000	0,41000	0,00000	0,64000	0,14800	0,45657	0,35285	0,83285
Melo et al.						CP_HDR			

Comparing the detection results obtained using the CP_HDR library with Melo et al. [12], we observed a considerable improvement in the UR metric. This means that the CP_HDR library detects more FPs across the image's brightest, intermediate, and darkest areas, while the Melo et al. implementation detected FPs only in the brightest and darkest areas, with no FP detected in the intermediate area.

V. CONCLUSIONS

In this study, we presented an investigation about the use of HDR images in FP detection and description. Initially, we made a systematic review with 21 studies. Only one study used HDR images, while the others used tone mapping algorithms to convert HDR images into LDR. Two studies presented datasets

that explore images with extreme lighting conditions, providing capture versions in LDR and HDR and metrics to evaluate detectors and descriptors.

In the previous implementation by Melo et al. [12], we have noticed some issues with code maintainability. So, we decided to rewrite it in order to provide a library called CP_HDR. We implemented the CP_HDR library to support both LDR and HDR images. It contains the complete SIFT algorithm (with subpixel precision, rotation invariance, and SIFT descriptor), the HfHDR and SfHDR proposed by Melo et al. [12]. In addition, new detector and descriptor algorithms can easily be added. We also implemented two image descriptors using Harris detector with SIFT descriptor (Harris+SIFT and HfHDR+SIFT), and an algorithm to segment images into groups of lighting intensities, that can be used to partition any image. All methods are documented, and there is a *Makefile* with examples of calls to execute the demonstration programs. The library is available on GitHub ³.

We observed that CP_HDR algorithms improved detection results when compared to Melo et al., especially with UR metric. Furthermore, most of the best results were obtained when using HDR images. This is a good indication that the use of HDR images provides better FP detection and description. HfHDR and SfHDR algorithms showed better UR values in most cases.

The CP_HDR library fulfills its purpose, showing improvement in UR and RR when compared to previous studies. HfHDR and SfHDR algorithms presented better detection performance when HDR images are used. The detected FPs are well distributed in all darkest, intermediate, and brightest areas of the image. In the description, SIFT algorithm performed better than the SfHDR. Thus, we consider that SfHDR and HfHDR achieve their goals as they improve FP detection in low-light areas. As future work, we may implement the SURF algorithm in CP_HDR, which was the one of the most used algorithm in the studies of the systematic review. We may also compare the use of LDR and HDR images with TM-LDR images and improving the CV filter and logarithmic mapping to generate less noise, especially in low-light areas and specular object surfaces.

CONFLICT OF INTEREST

The authors declare that they have no conflict of interest.

DATA AVAILABILITY

The code developed during the current study is available on GitHub ⁴.

REFERENCES

- [1] C. Schmid, R. Mohr, and C. Bauckhage, "Evaluation of interest point detectors," *International Journal of computer vision*, vol. 37, no. 2, pp. 151–172, 2000.
- [2] R. Szeliski, *Computer vision: algorithms and applications*. Springer Science & Business Media, 2010.
- [3] L. Chermak, N. Aouf, and M. Richardson, "HDR imaging for feature tracking in challenging visibility scenes," *Kybernetes*, vol. 43, no. 8, pp. 1129–1149, Jan 2014. [Online]. Available: <https://doi.org/10.1108/K-07-2014-0137>
- [4] B. T. Andrade, C. M. Mendes, J. de Oliveira Santos Jr, O. R. P. Bellon, and L. Silva, "3D preserving XVIII century Baroque masterpiece: Challenges and results on the digital preservation of Aleijadinho's sculpture of the Prophet Joel," *Journal of Cultural Heritage*, vol. 13, no. 2, pp. 210–214, 2012.
- [5] A. Rana, G. Valenzise, and F. Dufaux, "Evaluation of feature detection in HDR based imaging under changes in illumination conditions," in *2015 IEEE International Symposium on Multimedia (ISM)*, 2015, pp. 289–294.
- [6] C. Aguilera, F. Barrera, F. Lumbreras, A. D. Sappa, and R. Toledo, "Multispectral image feature points," *Sensors*, vol. 12, no. 9, pp. 12 661–12 672, 2012.
- [7] M. Hassaballah and A. I. Awad, *Detection and Description of Image Features: An Introduction*, 02 2016, vol. 630, ch. 1, pp. 1–8.
- [8] R. C. Gonzalez, R. E. Woods, and S. L. Eddins, *Digital image processing using MATLAB*. Pearson Education India, 2004.
- [9] E. Reinhard, W. Heidrich, P. Debevec, S. Pattanaik, G. Ward, and K. Myszkowski, *High dynamic range imaging: acquisition, display, and image-based lighting*. Morgan Kaufmann, 2010.
- [10] B. Příbyl, A. Chalmers, and P. Zemčík, "Feature point detection under extreme lighting conditions," in *Proceedings of the 28th Spring Conference on Computer Graphics*, 2012, pp. 143–150.
- [11] B. Příbyl, A. Chalmers, P. Zemčík, L. Hooberman, and M. Čadík, "Evaluation of feature point detection in high dynamic range imagery," *Journal of Visual Communication and Image Representation*, vol. 38, pp. 141–160, 2016.
- [12] W. A. L. J. de Melo, J. A. O. de Tavares, D. O. Dantas, and B. T. Andrade, "Improving feature point detection in high dynamic range images," in *2018 IEEE Symposium on Computers and Communications (ISCC)*. IEEE, 2018, pp. 00 091–00 096.
- [13] Y. Zhuang and L. Liang, "A novel local invariant feature extraction method for high-dynamic range images," in *2019 2nd International Conference on Safety Produce Informatization (IICSPI)*. IEEE, 2019, pp. 307–310.
- [14] R. Mukherjee, M. Bessa, P. Melo-Pinto, and A. Chalmers, "Object detection under challenging lighting conditions using high dynamic range imagery," *IEEE Access*, vol. 9, pp. 77 771–77 783, 2021.
- [15] A. S. Nascimento., W. A. L. de Jesus Melo., B. T. Andrade., and D. O. Dantas., "Evaluation of a local descriptor for HDR images," in *Proceedings of the 17th International Joint Conference on Computer Vision, Imaging and Computer Graphics Theory and Applications (VISIGRAPP 2022) - Volume 4: VISAPP, INSTICC*. SciTePress, 2022, pp. 299–306.
- [16] A. S. Nascimento, W. A. L. de Jesus Melo, D. O. Dantas, and B. T. Andrade, "Feature point detection in HDR images based on coefficient of variation," *Multimedia Tools and Applications*, Jul 2023. [Online]. Available: <https://doi.org/10.1007/s11042-023-16055-9>
- [17] K. Petersen, R. Feldt, S. Mujtaba, and M. Mattsson, "Systematic mapping studies in software engineering," in *12th International Conference on Evaluation and Assessment in Software Engineering (EASE) 12*, 2008, pp. 1–10.
- [18] B. Kitchenham, O. P. Brereton, D. Budgen, M. Turner, J. Bailey, and S. Linkman, "Systematic literature reviews in software engineering—a systematic literature review," *Information and software technology*, vol. 51, no. 1, pp. 7–15, 2009.
- [19] L. Chermak and N. Aouf, "Enhanced feature detection and matching under extreme illumination conditions with a HDR imaging sensor," in *2012 IEEE 11th International Conference on Cybernetic Intelligent Systems (CIS)*, 2012, pp. 64–69.
- [20] G. Kontogianni, E. Stathopoulou, A. Georgopoulos, and A. Doulamis, "HDR imaging for feature detection on detailed architectural scenes."

³Available at: https://github.com/ddantas-ufs/2024_cp_hdr. (Accessed on July 01, 2023)

⁴GitHub repository: https://github.com/ddantas-ufs/2024_cp_hdr.

- International Archives of the Photogrammetry, Remote Sensing & Spatial Information Sciences*, 2015.
- [21] R. Mantiuk, K. Myszkowski, and H.-P. Seidel, "A perceptual framework for contrast processing of high dynamic range images," *ACM Transactions on Applied Perception (TAP)*, vol. 3, pp. 286–308, 2006.
- [22] K. Jagadish and E. Sinzinger, "Image matching using high dynamic range images and radial feature descriptors," in *Advances in Visual Computing*, G. Bebis, R. Boyle, B. Parvin, D. Koracin, P. Remagnino, F. Porikli, J. Peters, J. Klosowski, L. Arns, Y. K. Chun, T.-M. Rhyne, and L. Monroe, Eds. Berlin, Heidelberg: Springer Berlin Heidelberg, 2008, pp. 359–369.
- [23] E. D. Sinzinger, "A model-based approach to junction detection using radial energy," *Pattern Recognition*, vol. 41, no. 2, pp. 494–505, 2008. [Online]. Available: <https://www.sciencedirect.com/science/article/pii/S0031320307003056>
- [24] L. Worthy and E. Sinzinger, "Scene identification using invariant radial feature descriptors," in *Eighth International Workshop on Image Analysis for Multimedia Interactive Services (WIAMIS '07)*, 2007, pp. 39–39.
- [25] E. O. Ige, K. Debattista, and A. Chalmers, "Towards HDR based facial expression recognition under complex lighting," in *Proceedings of the 33rd Computer Graphics International*, ser. CGI '16. New York, NY, USA: Association for Computing Machinery, 2016, p. 49–52. [Online]. Available: <https://doi.org/10.1145/2949035.2949048>
- [26] R. P. Kovalski and M. M. Oliveira, "High-quality reverse tone mapping for a wide range of exposures," in *2014 27th SIBGRAPI Conference on Graphics, Patterns and Images*, 2014, pp. 49–56.
- [27] Y. Huo, F. Yang, L. Dong, and V. Brost, "Physiological inverse tone mapping based on retina response," *The Visual Computer*, vol. 30, no. 5, pp. 507–517, May 2014. [Online]. Available: <https://doi.org/10.1007/s00371-013-0875-4>
- [28] G. Eilertsen, J. Kronander, G. Denes, R. K. Mantiuk, and J. Unger, "HDR image reconstruction from a single exposure using deep CNNs," *ACM Trans. Graph.*, vol. 36, no. 6, nov 2017. [Online]. Available: <https://doi.org/10.1145/3130800.3130816>
- [29] D. Marmerides, T. Bashford-Rogers, J. Hatchett, and K. Debattista, "ExpandNet: A deep convolutional neural network for high dynamic range expansion from low dynamic range content," *Computer Graphics Forum*, vol. 37, no. 2, pp. 37–49, 2018. [Online]. Available: <https://onlinelibrary.wiley.com/doi/abs/10.1111/cgf.13340>
- [30] S. Ren, K. He, R. Girshick, and J. Sun, "Faster R-CNN: Towards real-time object detection with region proposal networks," 2016.
- [31] W. Liu, D. Anguelov, D. Erhan, C. Szegedy, S. Reed, C.-Y. Fu, and A. C. Berg, "SSD: Single shot MultiBox detector," in *Computer Vision – ECCV 2016*. Springer International Publishing, 2016, pp. 21–37. [Online]. Available: https://doi.org/10.1007/978-3-319-46448-0_2
- [32] M. Everingham, L. Van Gool, C. K. I. Williams, J. Winn, and A. Zisserman, "The PASCAL Visual Object Classes Challenge 2007 (VOC2007) Results," <http://www.pascal-network.org/challenges/VOC/voc2007/workshop/index.html>.
- [33] —, "The PASCAL Visual Object Classes Challenge 2012 (VOC2012) Results," <http://www.pascal-network.org/challenges/VOC/voc2012/workshop/index.html>.
- [34] C. Harris, M. Stephens *et al.*, "A combined corner and edge detector," in *Alvey vision conference*, vol. 15. Citeseer, 1988, pp. 10–5244.
- [35] D. G. Lowe, "Distinctive image features from scale-invariant keypoints," *International journal of computer vision*, vol. 60, no. 2, pp. 91–110, 2004.
- [36] H. Bay, A. Ess, T. Tuytelaars, and L. Van Gool, "Speeded-up robust features (SURF)," *Computer vision and image understanding*, vol. 110, no. 3, pp. 346–359, 2008.
- [37] P. E. Debevec and J. Malik, "Recovering high dynamic range radiance maps from photographs," in *ACM SIGGRAPH 2008 classes*, 2008, pp. 1–10.
- [38] K. Zuiderveld, "Contrast limited adaptive histogram equalization," *Graphics gems*, pp. 474–485, 1994.
- [39] T. Ohdake and H. Chikatsu, "3D modelling of high relief sculpture using image-based integrated measurement system," *International Archives of the Photogrammetry, Remote Sensing and Spatial Information Sciences*, vol. 36, no. 5/W17, p. 6, 2005.
- [40] J. Shi *et al.*, "Good features to track," in *1994 Proceedings of IEEE conference on computer vision and pattern recognition*. IEEE, 1994, pp. 593–600.
- [41] E. Rosten and T. Drummond, "Fusing points and lines for high performance tracking," in *Tenth IEEE International Conference on Computer Vision (ICCV'05) Volume 1*, vol. 2. Ieee, 2005, pp. 1508–1515.
- [42] A. M. Reza, "Realization of the contrast limited adaptive histogram equalization (CLAHE) for real-time image enhancement," *Journal of VLSI signal processing systems for signal, image and video technology*, vol. 38, no. 1, pp. 35–44, 2004.
- [43] E. Reinhard and K. Devlin, "Dynamic range reduction inspired by photoreceptor physiology," *IEEE transactions on visualization and computer graphics*, vol. 11, no. 1, pp. 13–24, 2005.
- [44] R. Fattal, D. Lischinski, and M. Werman, "Gradient domain high dynamic range compression," in *Proceedings of the 29th annual conference on Computer graphics and interactive techniques*, 2002, pp. 249–256.
- [45] T. O. Aydin, R. Mantiuk, and H.-P. Seidel, "Extending quality metrics to full luminance range images," in *Human vision and electronic imaging xiii*, vol. 6806. International Society for Optics and Photonics, 2008, p. 68060B.
- [46] A. Rana, G. Valenzise, and F. Dufaux, "An evaluation of HDR image matching under extreme illumination changes," in *2016 Visual Communications and Image Processing (VCIP)*, 2016, pp. 1–4.
- [47] A. Alahi, R. Ortiz, and P. Vanderghenst, "Freak: Fast retina keypoint," in *2012 IEEE Conference on Computer Vision and Pattern Recognition*. Ieee, 2012, pp. 510–517.
- [48] S. Leutenegger, M. Chli, and R. Y. Siegwart, "Brisk: Binary robust invariant scalable keypoints," in *2011 International conference on computer vision*. Ieee, 2011, pp. 2548–2555.
- [49] A. Rana, G. Valenzise, and F. Dufaux, "Optimizing tone mapping operators for keypoint detection under illumination changes," in *2016 IEEE 18th International Workshop on Multimedia Signal Processing (MMSP)*, 2016, pp. 1–6.
- [50] —, "Learning-based adaptive tone mapping for keypoint detection," in *2017 IEEE International Conference on Multimedia and Expo (ICME)*, 2017, pp. 337–342.
- [51] K. Chiu, M. Herf, P. Shirley, S. Swamy, C. Wang, K. Zimmerman *et al.*, "Spatially nonuniform scaling functions for high contrast images," in *Graphics Interface*. Canadian Information Processing Society, 1996, pp. 245–245.
- [52] F. Drago, K. Myszkowski, T. Annen, and N. Chiba, "Adaptive logarithmic mapping for displaying high contrast scenes," in *Computer graphics forum*, vol. 22, no. 3. Wiley Online Library, 2003, pp. 419–426.
- [53] A. Rana, G. Valenzise, and F. Dufaux, "Learning-based tone mapping operator for image matching," in *2017 IEEE International Conference on Image Processing (ICIP)*, Sep. 2017, pp. 2374–2378.
- [54] —, "Learning-based tone mapping operator for efficient image matching," *IEEE Transactions on Multimedia*, vol. 21, no. 1, pp. 256–268, 2019.
- [55] C.-H. Yeh and M.-H. Lin, "Robust 3D reconstruction using HDR-based SLAM," *IEEE Access*, vol. 9, pp. 16 568–16 581, 2021.
- [56] R. A. Newcombe, S. Izadi, O. Hilliges, D. Molyneaux, D. Kim, A. J. Davison, P. Kohi, J. Shotton, S. Hodges, and A. Fitzgibbon, "Kinectfusion: Real-time dense surface mapping and tracking," in *2011 10th IEEE international symposium on mixed and augmented reality*. Ieee, 2011, pp. 127–136.
- [57] J. Sturm, N. Engelhard, F. Endres, W. Burgard, and D. Cremers, "A benchmark for the evaluation of RGB-D SLAM systems," in *2012 IEEE/RSJ international conference on intelligent robots and systems*. IEEE, 2012, pp. 573–580.

- [58] R. Mur-Artal and J. D. Tardós, "ORB-SLAM2: An open-source SLAM system for monocular, stereo, and RGB-D cameras," *IEEE transactions on robotics*, vol. 33, no. 5, pp. 1255–1262, 2017.
- [59] A. Albrecht and N. F. Heide, "Improving feature-based visual SLAM in person indoor navigation with HDR imaging," in *2019 IEEE 2nd International Conference on Information Communication and Signal Processing (ICICSP)*, Sep. 2019, pp. 369–373.
- [60] T. Mertens, J. Kautz, and F. Van Reeth, "Exposure fusion," in *15th Pacific Conference on Computer Graphics and Applications (PG'07)*, 2007, pp. 382–390.
- [61] T. Jinno, S. Kuriyama, and M. Okuda, "Tone-mapping for an HDR surveillance system using SIFT features," in *21st European Signal Processing Conference (EUSIPCO 2013)*, 2013, pp. 1–5.
- [62] E. Reinhard, M. Stark, P. Shirley, and J. Ferwerda, "Photographic tone reproduction for digital images," in *Proceedings of the 29th Annual Conference on Computer Graphics and Interactive Techniques*, ser. SIGGRAPH '02. New York, NY, USA: Association for Computing Machinery, 2002, p. 267–276. [Online]. Available: <https://doi.org/10.1145/566570.566575>
- [63] Y. Li, L. Sharan, and E. H. Adelson, "Compressing and companding high dynamic range images with subband architectures," *ACM Trans. Graph.*, vol. 24, no. 3, p. 836–844, Jul. 2005. [Online]. Available: <https://doi.org/10.1145/1073204.1073271>
- [64] G. W. Larson, H. Rushmeier, and C. Piatko, "A visibility matching tone reproduction operator for high dynamic range scenes," *IEEE Transactions on Visualization and Computer Graphics*, vol. 3, no. 4, pp. 291–306, 1997.
- [65] M. Ashikhmin, "A tone mapping algorithm for high contrast images," in *Proceedings of the 13th Eurographics Workshop on Rendering*, ser. EGRW '02. Goslar, DEU: Eurographics Association, 2002, p. 145–156.
- [66] S. Pattanaik and H. Yee, "Adaptive gain control for high dynamic range image display," in *Proceedings of the 18th Spring Conference on Computer Graphics*, ser. SCCG '02. New York, NY, USA: Association for Computing Machinery, 2002, p. 83–87. [Online]. Available: <https://doi.org/10.1145/584458.584472>
- [67] C. Schlick, "An adaptive sampling technique for multidimensional integration by ray-tracing," in *Photorealistic Rendering in Computer Graphics*, P. Brunet and F. W. Jansen, Eds. Berlin, Heidelberg: Springer Berlin Heidelberg, 1994, pp. 21–29.
- [68] R. Mantiuk, S. Daly, and L. Kerofsky, "Display adaptive tone mapping," *ACM Trans. Graph.*, vol. 27, no. 3, p. 1–10, Aug. 2008. [Online]. Available: <https://doi.org/10.1145/1360612.1360667>
- [69] R. Fattal, "Edge-avoiding wavelets and their applications," *ACM Trans. Graph.*, vol. 28, no. 3, Jul. 2009. [Online]. Available: <https://doi.org/10.1145/1531326.1531328>
- [70] C. Kiser, E. Reinhard, M. Tocci, and N. Tocci, "Real time automated tone mapping system for HDR video," in *IEEE International Conference on Image Processing*, vol. 134. IEEE Orlando, FL, 2012.
- [71] R. Yates and R. Lyons, "DC blocker algorithms [DSP tips & tricks]," *IEEE Signal Processing Magazine*, vol. 25, no. 2, pp. 132–134, 2008.
- [72] F. Durand and J. Dorsey, "Fast bilateral filtering for the display of high-dynamic-range images," in *Proceedings of the 29th annual conference on Computer graphics and interactive techniques*, 2002, pp. 257–266.
- [73] A. Chalmers and K. Debattista, "HDR video past, present and future: A perspective," *Signal Processing: Image Communication*, vol. 54, pp. 49–55, 2017. [Online]. Available: <https://www.sciencedirect.com/science/article/pii/S092359651730019X>
- [74] P. Ledda, A. Chalmers, T. Troscianko, and H. Seetzen, "Evaluation of tone mapping operators using a high dynamic range display," *ACM Trans. Graph.*, vol. 24, no. 3, p. 640–648, Jul. 2005. [Online]. Available: <https://doi.org/10.1145/1073204.1073242>
- [75] M. Čadík, M. Wimmer, L. Neumann, and A. Artusi, "Evaluation of HDR tone mapping methods using essential perceptual attributes," *Computers & Graphics*, vol. 32, no. 3, pp. 330–349, 2008. [Online]. Available: <https://www.sciencedirect.com/science/article/pii/S0097849308000460>
- [76] K. Mikolajczyk and C. Schmid, "A performance evaluation of local descriptors," *IEEE transactions on pattern analysis and machine intelligence*, vol. 27, no. 10, pp. 1615–1630, 2005.
- [77] B. S. Everitt and A. Skrondal, *The Cambridge dictionary of statistics*. New York: Cambridge University Press, 2010.